Supporting Information

Bulk-to-surface Co-modification of Layered Hydrated Vanadate Cathode for Aqueous Zinc Ion Batteries

Chen Zhang [a], Yan Huang [b], Xueer Xu [a], Ziyu Chen [a], Gang Xiao [b], Yu Zhong [a], Xiuli Wang [a], Changdong Gu [a]*, and Jiangping Tu [a]

a. State Key Laboratory of Silicon Materials Key Laboratory of Advanced Materials and Applications for Batteries of Zhejiang Province and School of Materials Science and Engineering Zhejiang University Hangzhou 310027, China. E-mail: cdgu@zju.edu.cn

b. State Key Laboratory of Clean Energy Utilization, College of Energy Engineering, Zhejiang University, Hangzhou, Zhejiang 310027, China

Experimental section

Synthesis of CaNaVO-44

All chemicals were analytically pure reagents and can be used without further purification. CaNaVO-44 nanoribbons were prepared by a simple hydrothermal method. First, V_2O_5 (6 mmol) was dispersed into deionized water (60 ml), followed by the addition of H_2O_2 (5 ml, 30%) and stirring for 30 min. Then, $Ca(NO_3)_2{\cdot}4H_2O$ (4 mmol) and NaOH (4 mmol) were added to the above solution. After stirring for 30 min, the above solution was transferred to a 100 ml Teflon-lined autoclave and heated at 180°C for 32 h. After cooling to room temperature, the final sample was collected and washed three times each with anhydrous ethanol and deionized water, respectively. The final powders were obtained by freeze-drying and named CaNaVO-44. Comparison samples were prepared using the same method. The total amount of $Ca(NO_3)_2{\cdot}4H_2O$ and NaOH added was 8 mmol, and the samples CaNaVO-17, CaNaVO-26, CaNaVO-35 and CaNaVO-53 were synthesized according to the different ratios of $Ca(NO_3)_2{\cdot}4H_2O$ and NaOH added. For comparison, a sample with only $Ca(NO_3)_2{\cdot}4H_2O$ (4 mmol) or NaOH (4 mmol) added to each was noted as NaVO-4 or CaVO-4. The sample without $Ca(NO_3)_2{\cdot}4H_2O$ and NaOH added were noted as VO.

Synthesis of CaKVO-26

The same method was used to prepare CaKVO-26. First, V_2O_5 (6 mmol) was dispersed into deionized water (60 ml), followed by the addition of H_2O_2 (5 ml, 30%) and stirring for 30 min. Then, $Ca(NO_3)_2{\cdot}4H_2O$ (2 mmol) and KOH (6 mmol) were added to the above solution. After stirring for 30 min, the above solution was transferred to a 100 ml Teflon-lined autoclave and heated at 180°C for 32 h. After cooling to room temperature, the final products were collected and washed three times each with anhydrous ethanol and deionized water, respectively. The final powders were obtained by freeze-drying and named CaKVO-26. Comparison samples were prepared using the same method. The total amount of $Ca(NO_3)_2{\cdot}4H_2O$ and KOH added was 8 mmol, and the samples CaKVO-17, CaKVO-35, and CaKVO-44 were synthesized according to the different ratios of $Ca(NO_3)_2{\cdot}4H_2O$ and KOH added.

Synthesis of BaKVO-17

The same method was used to prepare BaKVO-26. First, V_2O_5 (6 mmol) was dispersed into deionized water (60 ml), followed by the addition of H_2O_2 (5 ml) and stirring for 30 min. Then, $Ba(NO_3)_2{\cdot}4H_2O$ (1 mmol) and KOH (7 mmol) were added to the above solution. After stirring for 30 min, the above solution was transferred to a 100 ml Teflon-lined autoclave and heated at 180°C for 32 h. After cooling to room temperature, the final products were collected and washed three times each with anhydrous ethanol and deionized water, respectively. The final powders were obtained by freeze-drying and named BaKVO-17. Comparison samples were prepared using the same method. The total amount of $Ba(NO_3)_2{\cdot}4H_2O$ and KOH added was 8 mmol, and the samples BaKVO-26, BaKVO-35, and BaKVO-44 were synthesized according to the different ratios of $Ba(NO_3)_2{\cdot}4H_2O$ and KOH added.

Material characterization

Powder X-ray diffraction (XRD) was employed to analyze the crystal structure of the samples (RIGAKU D/MAX 2550/PC, Cu Kα radiation, λ = 1.54178 Å). Field emission scanning electron microscope (FESEM, Gemini SEM 300) and transmission electron microscope (TEM, JEM 2100F) were used to observe the morphology and dimensions of the samples. The elemental composition of samples underwent measurement through the utilization of X-ray photoelectron spectroscopy (XPS, Thermo Scientific, K-Alpha). Molecular vibrational states were analyzed by microscopic laser Raman spectrometer (Raman, Horiba Lab RAM HR Evolution) and Fourier transform infrared spectroscopy (FTIR, Thermo Scientific Nicolet iS20). The thermogravimetric analysis (TG, TA SDT Q600) was conducted in air with a temperature range of 30 °C to 500 °C at a 10 °C·min^{-1}. The inductively coupled plasma optical emission spectrometer (ICP-OES, Agilent 730) was used to determine elemental contents.

Electrochemical measurement

CR2025-type coin cells were used for all electrochemical measurements. The active substance, super P and polyvinylidene fluoride (PVDF) binder were mixed with N-methyl-2-pyrrolidone (NMP) solvent to form a homogeneous slurry in a weight ratio of 7:2:1 to obtain the working electrode. The paste was subsequently coated onto a Ti foil (200 μm) and then dried under vacuum oven conditions at 60°C for 12 h. The resulting electrode was ultimately cut into discs with a 15 mm diameter. The total weight of the active substance on the working electrodes was trolled to be around 1 mg cm^{-2}. The AZIBs were assembled using metallic zinc foil (Φ = 15 mm) as the anode and glass fiber (GF/F, Whatman) as the separator. The electrolyte comprised an aqueous solution of 3 M $Zn(CF_3SO_3)_2$ and 0.1 M Na_2SO_4. To carry out in situ electrochemical conversion of Zn||CaNaVO-44 cells, the new cells were first charged to 1.6 V at a current density of 0.1 A g^{-1}. All duration charge/discharge tests were carried out on the LAND battery test system. The range of test voltage was from 0.2 to 1.6 V (vs. Zn/Zn^{2+}). Cyclic voltammetry (CV) measurements of the full cells (0.1~1.0 mV s^{-1}, 0.2~1.6 V, vs. Zn/Zn^{2+}) were conducted with a CHI660E electrochemical workstation (Shanghai Chenhua Co., Ltd.). Electrochemical impedance spectroscopy (EIS) was conducted in the frequency range of 100 kHz to 0.1 Hz using a current amplitude of 10 mV on the Princeton PARSTAT MC 1000 electrochemical workstation. The full cells were tested using the constant current intermittent titration technique (GITT) at a current density of 50 mA g^{-1} with a constant current discharge pulse of 10 min and a relaxation time of 30 min per step on the LAND battery test system.

DFT calculations

Density Functional Theory (DFT) calculations in this paper were performed using the Vienna Ab-initio Simulation Package (VASP), along with Perdew, Burke, and Ernzerhof (PBE) formulas in the Generalized Gradient Approximation (GGA).[1,, 2] The Projected Augmented Wave (PAW) method has been used to represent the electron in the nucleus.[3] For structural optimization, we utilized the Monkhorst-Pack methods having 0.04 A^{-1} density for sampling. Consider that the electron energy was self-consistent for energy changes below 10^{-4} eV. The cut-off energy was set to 520 eV, and the ion force was optimized until it was less than 0.03 eV A^{-1}. To accurately handle the strong electron correlation effects in V, the DFT+U method was used, where U_V=3.25 eV.[4] The climbing-image nudged elastic band (CI-NEB) method was utilized to calculate the energy barriers for ion diffusion.[5] The spacing between the vacuum and the plane of the structure was 20 Å. The Brillouin zone integral used the surface structures of 5 × 2 × 1 Monkhorst pack K-point sampling. The adsorption energies (E_{ads}) were calculated as $E_{ads} = E_{ad/sub} - E_{ad} - E_{sub}$, where $E_{ad/sub}$, E_{ad}, and E_{sub} correspond to the optimized adsorbate/substrate system, the adsorbate in the structure, and the clean substrate, respectively. To maintain a similar stoichiometry to $Ca_{0.56}Na_{1.19}V_6O_{16}\cdot 4.09H_2O$ and $V_5O_{12}\cdot 2.39H_2O$, we constructed $Ca_{0.5}NaV_6O_{16}\cdot 4H_2O$ and $V_5O_{12}\cdot 2.4H_2O$ models for DFT calculations.

The equilibrium voltage was calculated from the internal energy calculated by DFT, The cathode voltage equation for Zn^{2+} in $Ca_{0.5}NaV_6O_{16}\cdot 4H_2O$ is as follows：

$$V_{Zn} = \frac{E(Zn_{x_1}Ca_{0.5}NaV_6O_{16}\cdot 4H_2O - E\left(Zn_{x_2}Ca_{0.5}NaV_6O_{16}\cdot 4H_2O\right) - (X_2 - X_1)E(Zn)}{2(X_2 - X_1)F}$$

The cathode voltage equation for H^+ in $Ca_{0.5}NaV_6O_{16}\cdot 4H_2O$ is as follows：

$$V_H = \frac{E(H_{x_1}Ca_{0.5}NaV_6O_{16}\cdot 4H_2O - E\left(H_{x_2}Ca_{0.5}NaV_6O_{16}\cdot 4H_2O\right) - (X_2 - X_1)E(H)}{(X_2 - X_1)F}$$

Supplementary Methods

Method S1: Calculation of Energy Density and Power Density

The energy density (*E*, Wh kg^{-1}) and power density (*P*, kg^{-1}) of Zn||CaNaVO-44@CS cells were determined according to the following methodology.[6]

$$E = \int_0^t \frac{IV(t)dt}{\mathrm{M}}$$

$$P = \frac{E \times 3600}{t}$$

Where *I* (A) and *V* (V) represent the current and voltage of the cell, respectively, *t* (s) indicates the discharge time, and *M* (g) represents the weight of the active substance.

Method S2: Calculation of Capacitance and Diffusion Control Contributions

The peak response current (*i*, mA) and scan rate can (*v*, mV s^{-1}) be fitted for different scan rates using the following equation.[7]

$$i = \mathrm{a}v^b$$

Where *i* is the peak current (mA), *v* is the scan rate (mV s^{-1}) and a and *b* are constants. The capacitance contribution can be analyzed qualitatively by the power law relationship between *v* and *i*.

The current (*i*, mA) at a certain potential can be divided into capacitance-limited (k_1v) and diffusion-limited effects ($k_2v^{1/2}$) as shown in the following equation.[8]

$$i = \mathrm{k}_1 v + \mathrm{k}_2 v^{1/2}$$

Method S3: Calculation of Ion Diffusion Coefficient

D can be calculated according to the following equation:[9]

$$D = \frac{4}{\pi\tau}\left(\frac{\mathrm{m_B V_M}}{\mathrm{SM_B}}\right)^2\left(\frac{\Delta E_S}{\Delta E_\tau}\right)^2$$

Where τ represents the pulse duration (s), m_B denotes the mass of the active substance (g), M_B and V_M indicate the molar mass (g mol^{-1}) and molar volume (cm^3 mol^{-1}), respectively. S represents the contact area (cm^2) between the electrode and the electrolyte, *ΔEs*, and *ΔEτ* represent the voltage changes (V) in steady-state conditions and under the influence of a constant current pulse, respectively.

Method S4: Calculation of distribution of relaxation times (DRT) method

The DRT method is a mathematical transformation that converts Nyquist plots from the frequency domain into DRT profiles in the time domain.[10]

$$Z_{DRT} = R_\infty + \int_{-\infty}^{\infty} \frac{\gamma(ln\tau)}{1 + \mathrm{i}2\pi} dln\tau$$

Method S5: Calculation of Energy Efficiency and Charge/Discharge Voltage Difference

The energy efficiency (*EE*, %) and charge/discharge voltage difference (Voltage difference, V) can be calculated according to the following equation.[11]

$$EE = \frac{Discharge\ energy}{Charge\ energy} = \frac{Coulombic\ efficiency \times (1 - Voltage\ difference)}{Charge\ voltage}$$

$$Voltage\ difference = Charge\ voltage - Discharge\ voltage$$

Where both the discharge (V) and charge voltage (V) are the median voltages on the discharge and charge curves.

Supplementary Figures

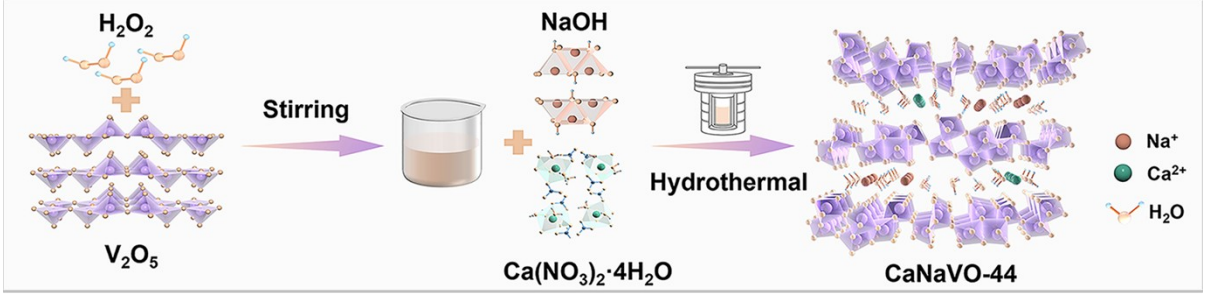

Figure S1. Schematic of CaNaVO-44 sample synthesis.

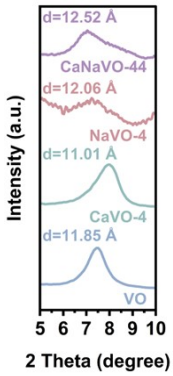

Figure S2. XRD local magnification pattern s of CaNaVO-44, NaVO-4, CaVO-4, and VO.

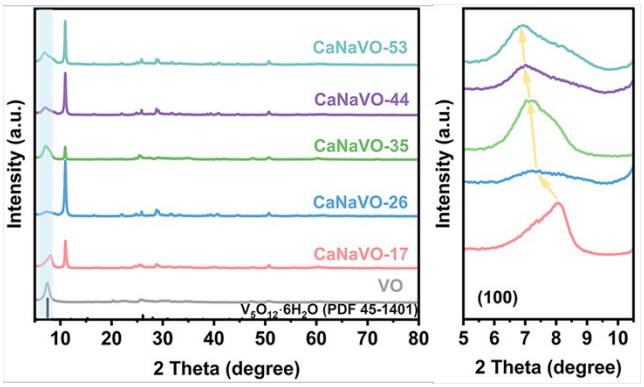

Figure S3. XRD patterns of samples with different Na^+ and Ca^{2+} addition ratios.

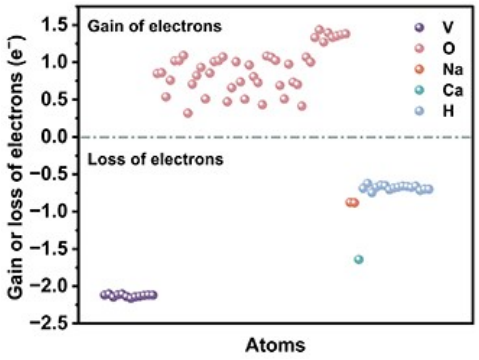

Figure S4. Electron gain/loss of different atoms calculated by Bader charge analysis.

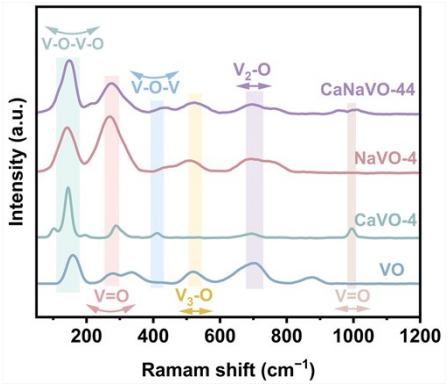

Figure S5. Raman spectra of CaNaVO-44, NaVO-4, CaVO-4 and VO.

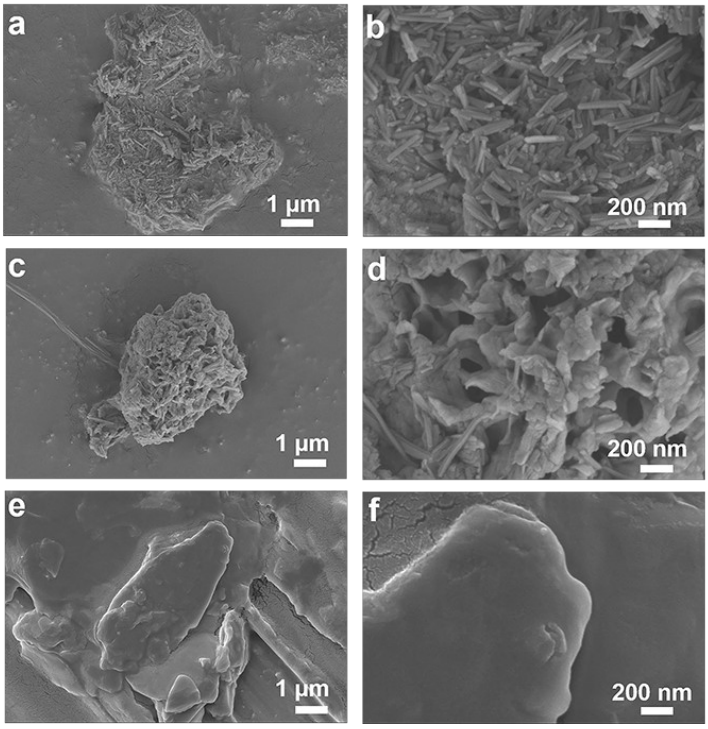

Figure S6. SEM images of (a, b) NaVO-4, (c, d) CaVO-4, and (e, f) VO.

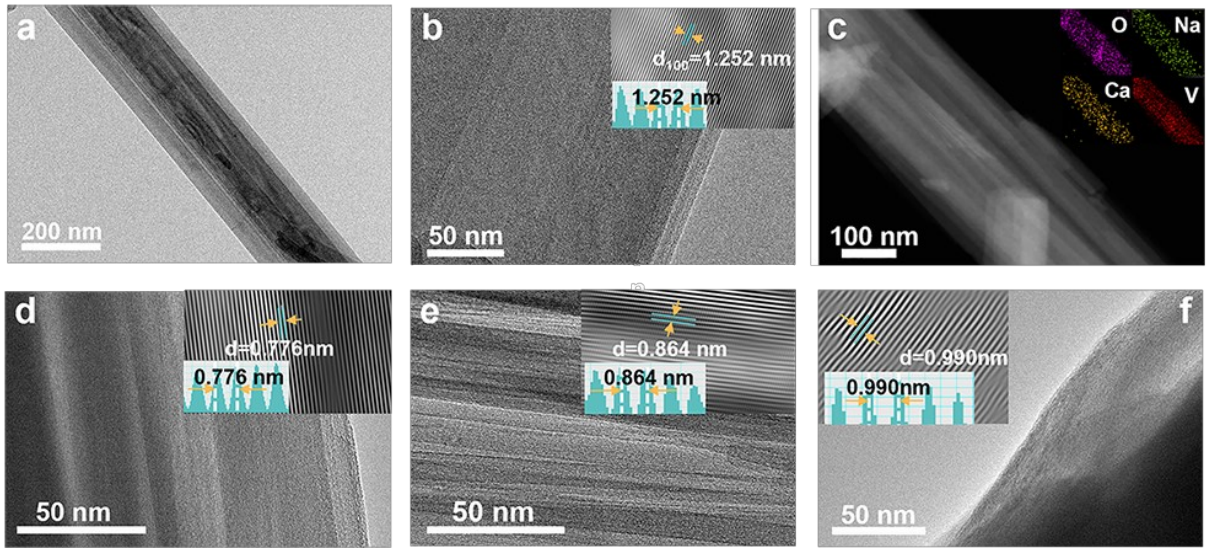

Figure S7. (a, b) TEM images, and (c) EDS mapping of CaNaVO-44. TEM images of (d) NaVO-4, (e) CaVO-4 and (f) VO.

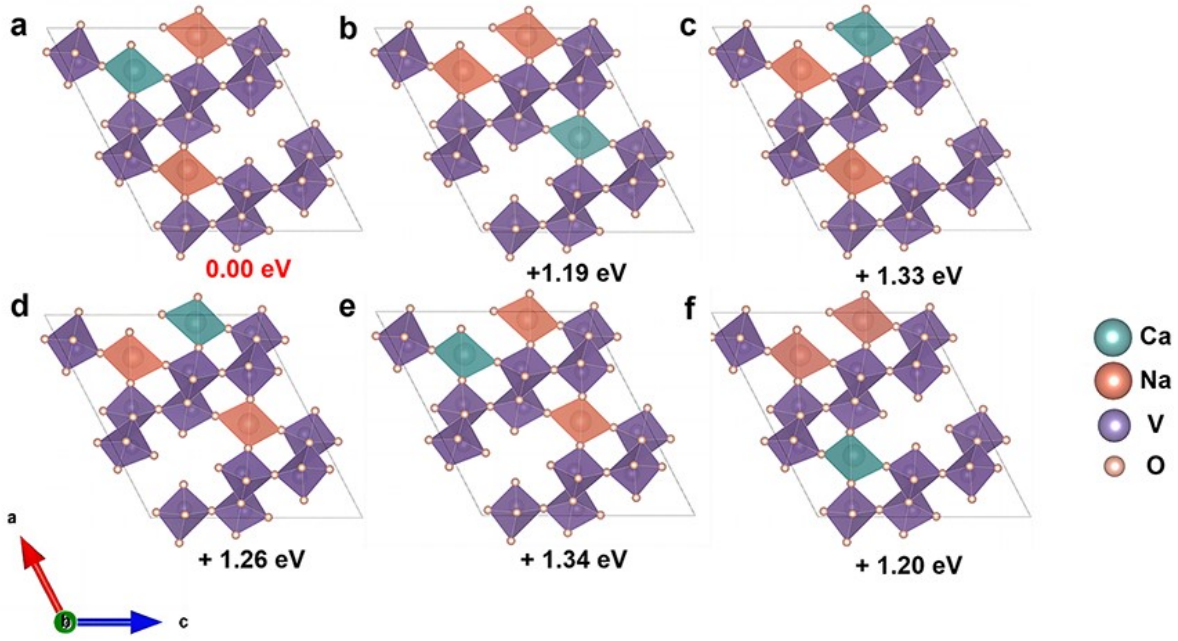

Figure S8. Structural optimization of $Ca_{0.5}NaV_6O_{16}$.

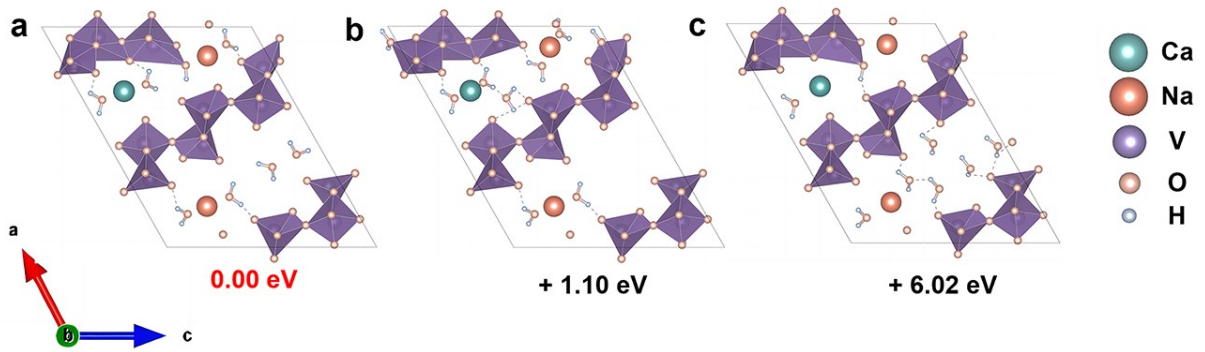

Figure S9. Structural optimization of $Ca_{0.5}NaV_6O_{16}\cdot 4H_2O$.

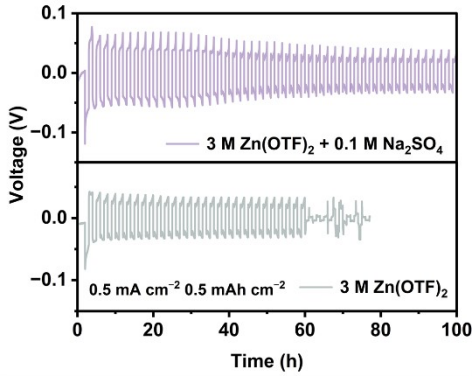

Figure S10. Stripping/plating stability of Zn||Zn symmetric cells using 3 M $Zn(OTF)_2$ + 0.1 M Na_2SO_4 and 3 M $Zn(OTF)_2$ electrolytes at 0.5 mA cm^{-2} and a capacity of 0.5 mAh cm^{-2}.

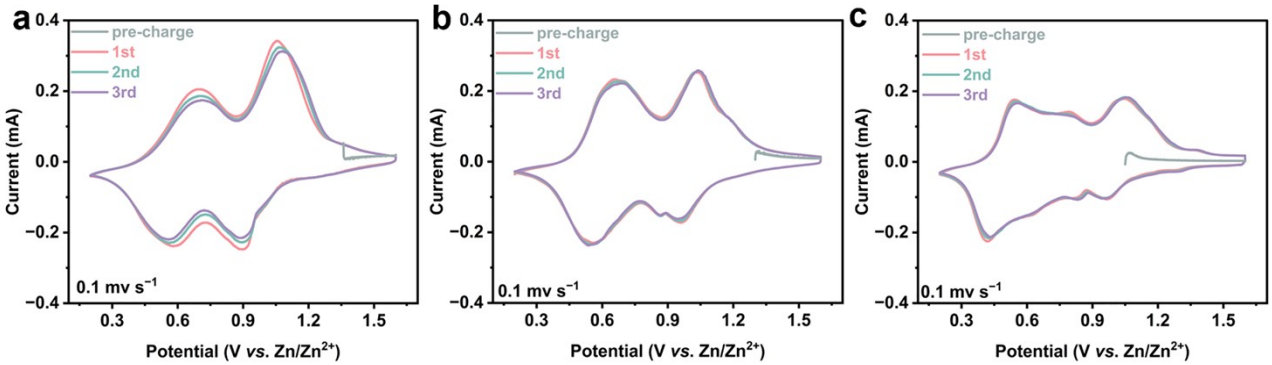

Figure S11. CV curves of (a) Zn||NaVO-4, (b) Zn||CaVO-4@CS, and (c) Zn||VO cells.

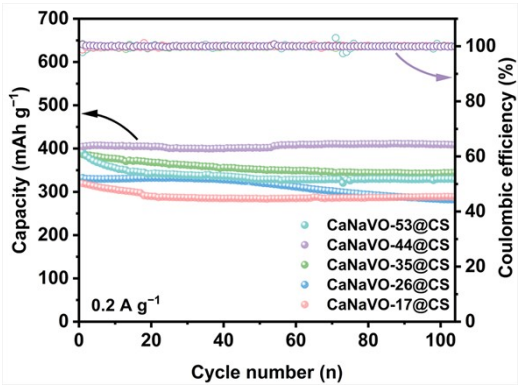

Figure S12. Cycling performance at 0.2 A g^{-1} of cathodes with different Na^{+} and Ca^{2+} addition ratios.

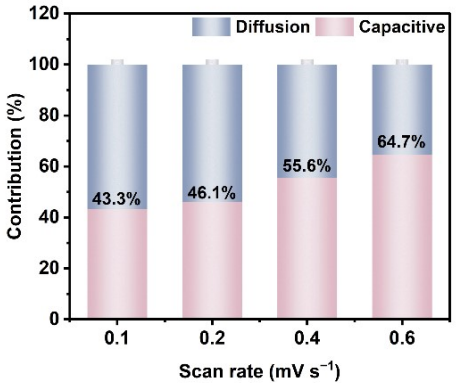

Figure S13. Capacitance contribution at different scan rates for VO cathode.

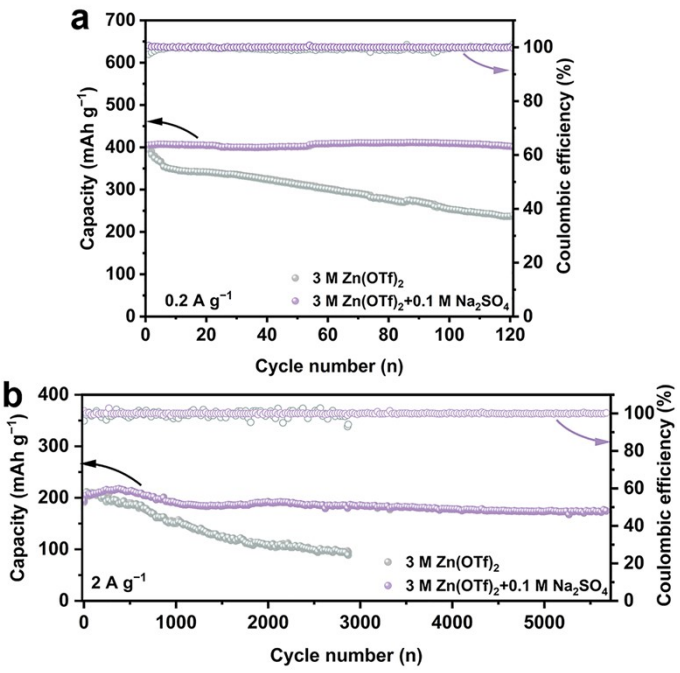

Figure S14. Cycling performance of Zn||CaNaVO-44 cells with and without Na_2SO_4 at (a) 0.2 A g^{-1} and (b) 2.0 A g^{-1}.

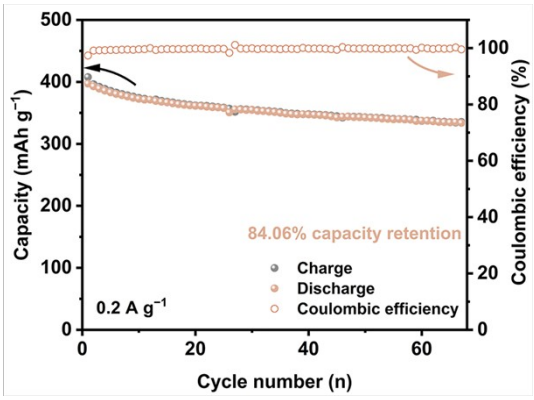

Figure S15. Cycling performance at 0.2 A g^{-1} for the Zn||CaNaVO-44@CS cell using 3 M $Zn(OTF)_2$ and 0.1 M $ZnSO_4$ as electrolyte.

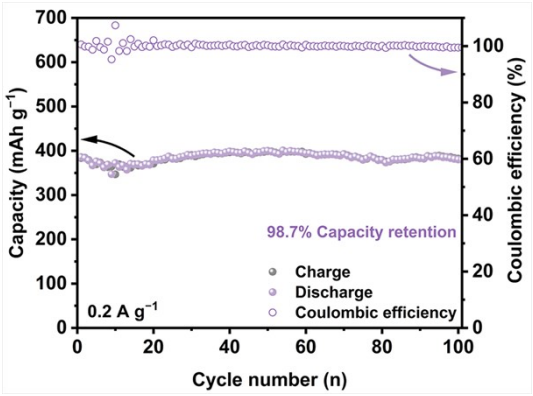

Figure S16. Cycling performance at 0.2 A g^{-1} for the Zn||CaNaVO-44@CS cell using 3 M $Zn(ClO_4)_2$ and 0.1 M Na_2SO_4 as electrolyte.

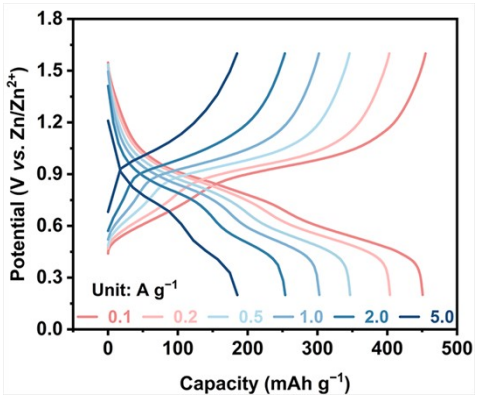

Figure S17. GCD curves at different current densities of Zn||CaNaVO-44@CS cell.

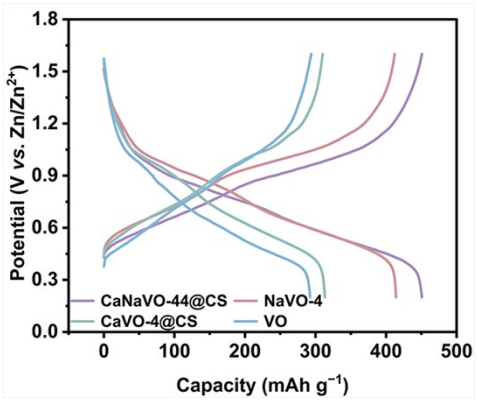

Figure S18. GCD curves at 0.1 A g^{-1} of CaNaVO-44@CS, NaVO-4, CaVO-4@CS, and VO cathodes.

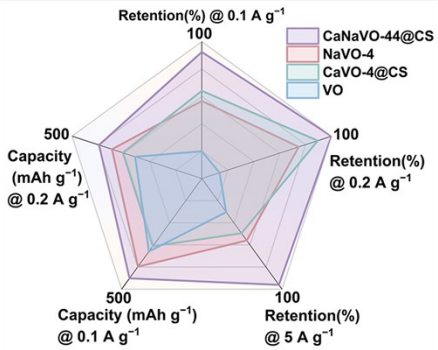

Figure S19. Comparison of electrochemical properties of CaNaVO-44@CS, NaVO-4, CaVO-4@CS, and VO cathodes.

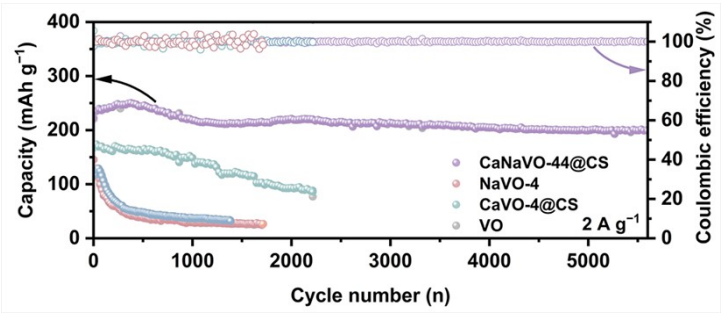

Figure S20. Cycling performance at 2.0 A g^{-1} of CaNaVO-44@CS, NaVO-4, CaVO-4@CS, and VO cathodes.

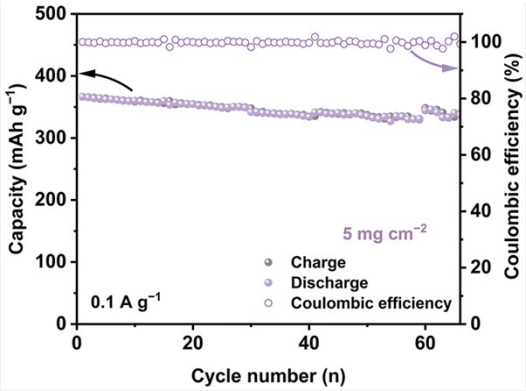

Figure S21. Cycling performance at 0.1 A g^{-1} for the Zn||CaNaVO-44@CS cell at an active substance loading of 5 mg cm^{-2}.

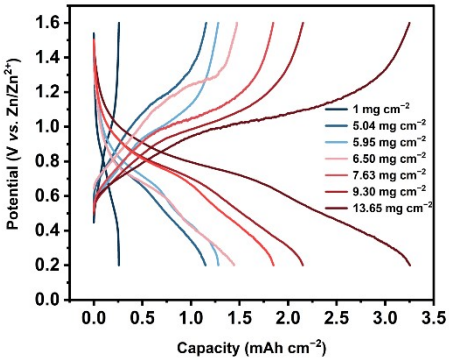

Figure S22. Areal capacities of the CaNaVO-44@CS cathodes at 0.1 A g^{-1} for different active substance masses.

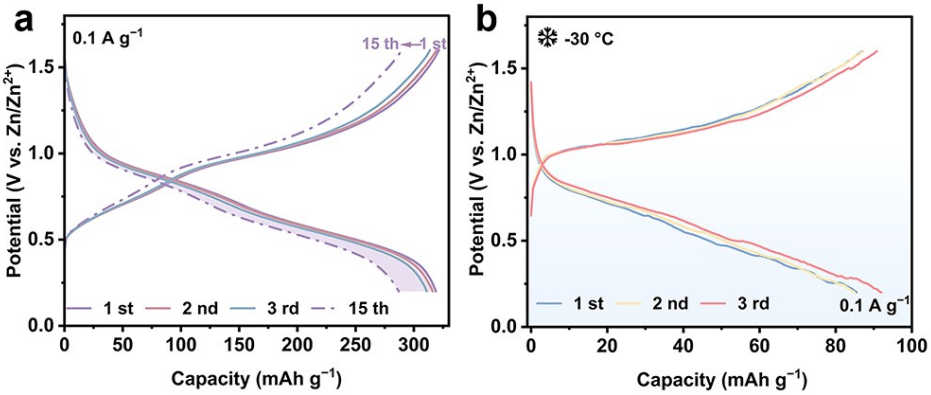

Figure S23. GCD curves of Zn||CaNaVO-44@CS pouch cells at 0.1 A g^{-1} under conditions of 25 and -30 °C.

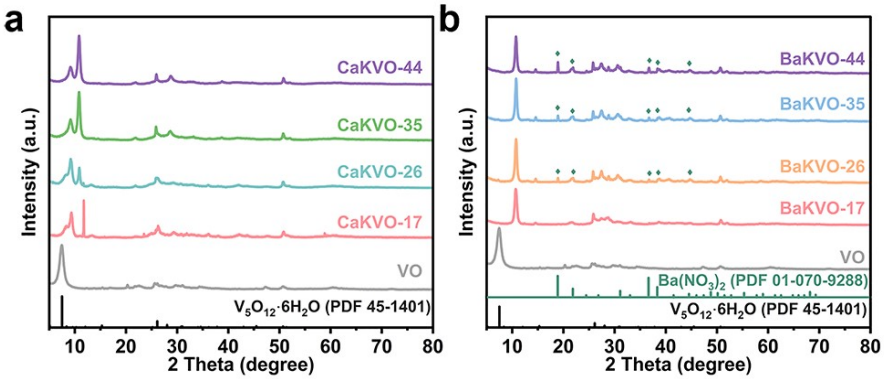

Figure S24. XRD patterns of samples with different (a) K^+ and Ca^{2+}, and (b) K^+ and Ba^{2+} addition ratios.

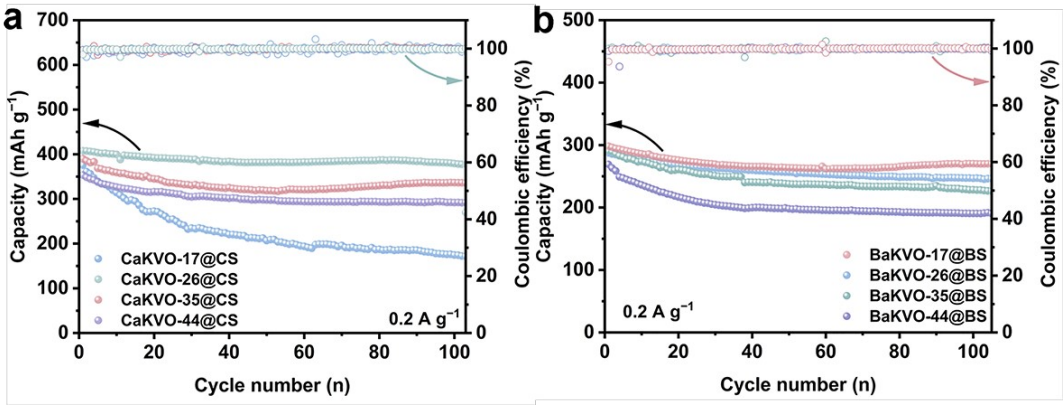

Figure S25. Cycling performance at 0.2 A g^{-1} of cathodes with different (a) K^+ and Ca^{2+}, and (b) K^+ and Ba^{2+} addition ratios.

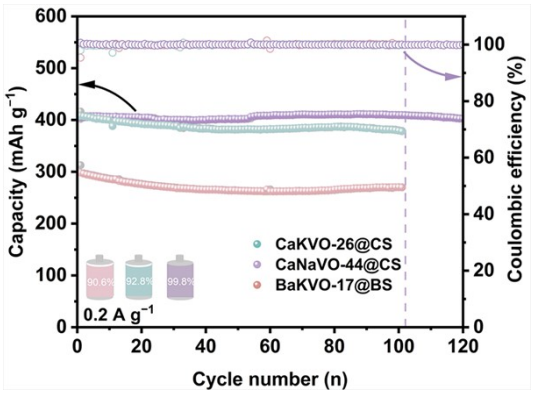

Figure S26. Cycling performance at 0.2 A g^{-1} of CaKVO-26@CS, BaKVO-17@BS, and CaNaVO-44@CS cathodes.

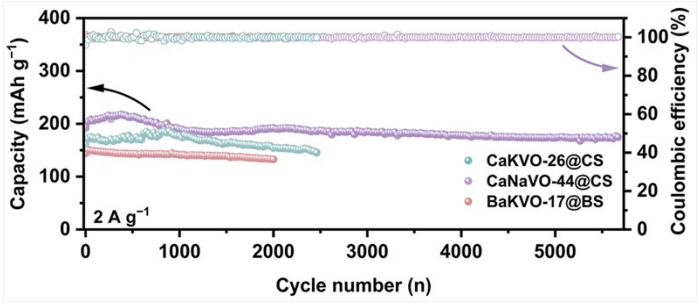

Figure S27. Cycling performance at 2.0 A g^{-1} of CaKVO-26@CS, BaKVO-17@BS, and CaNaVO-44@CS cathodes.

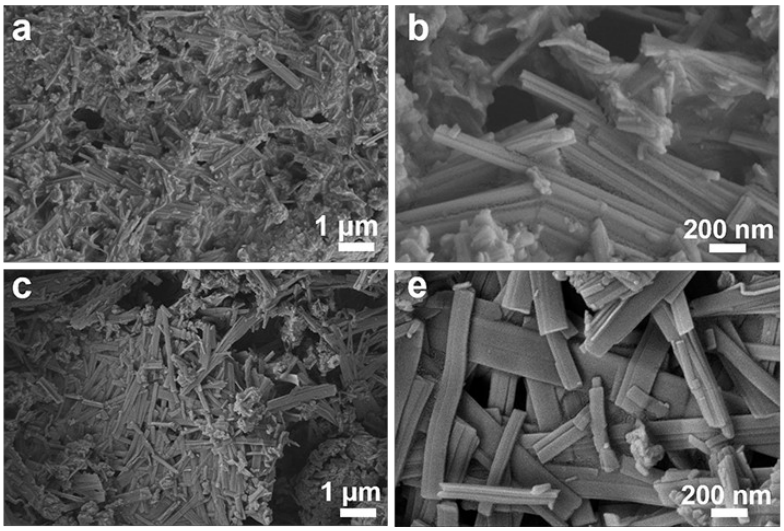

Figure S28. SEM images of (a, b) CaKVO-26, and (c, d) BaKVO-17.

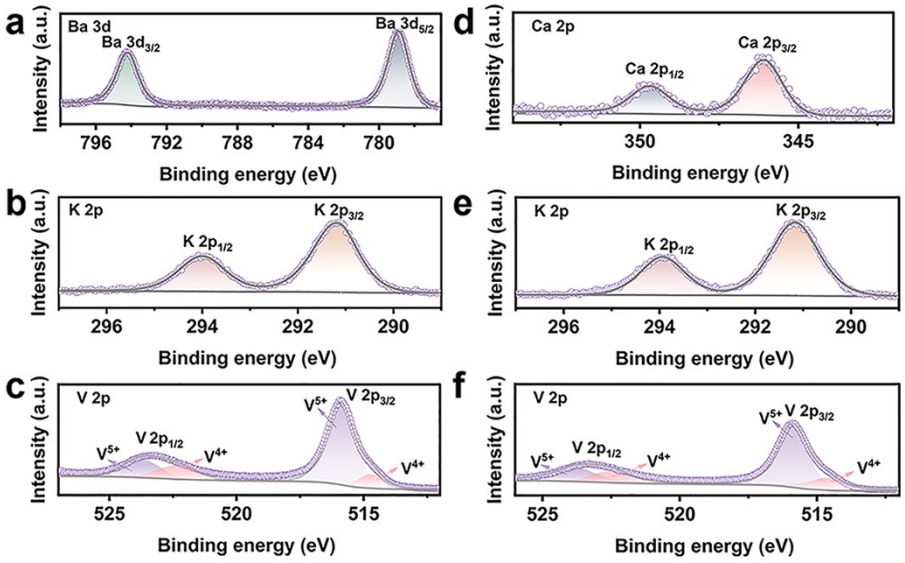

Figure S29. XPS spectrums of Ba 3d (a), K 2p (b), and V 2p (c) of CaKVO-26. XPS spectrums of Ca 2p (d), K 2p (e), and V 2p (f) of BaKVO-17.

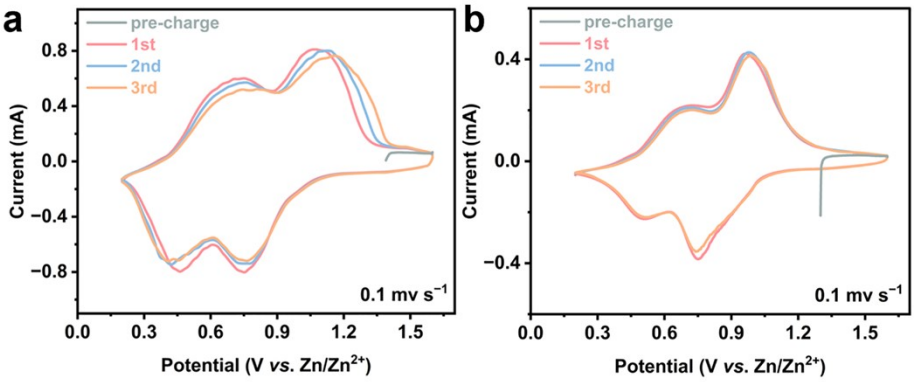

Figure S30. CV curves of (a) Zn||CaKVO-26@CS, and (b) Zn||BaKVO-17@BS cells.

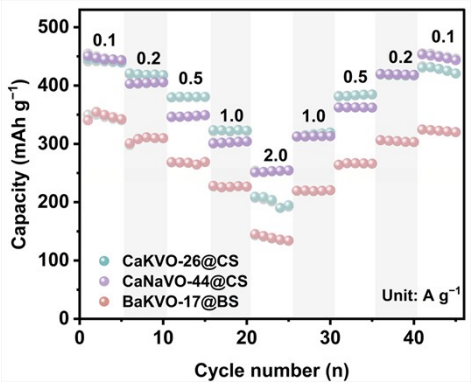

Figure S31. Rate performance of CaKVO-26@CS, BaKVO-17@BS, and CaNaVO-44@CS cathodes.

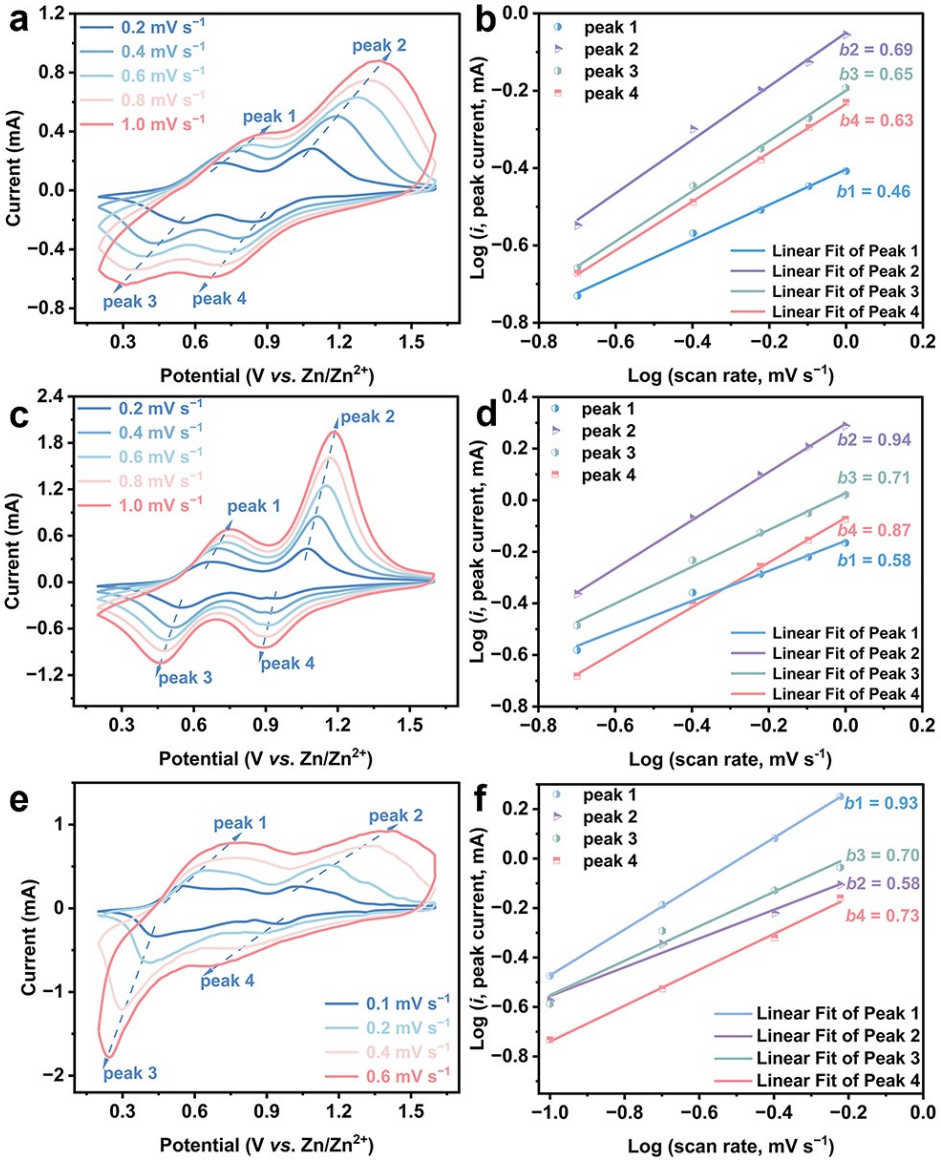

Figure S32. CV curves at different scan rates of (a) NaVO-4, (c) CaVO-4@CS, and (e) VO cathodes. Peak current versus scan rate of (b) NaVO-4, (d) CaVO-4@CS, and (f) VO cathodes.

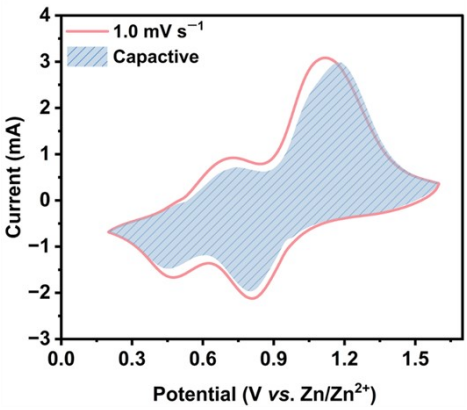

Figure S33. CV curve of the CaNaVO-44@CS cathode with capacity separation at 1.0 mV s^{-1}.

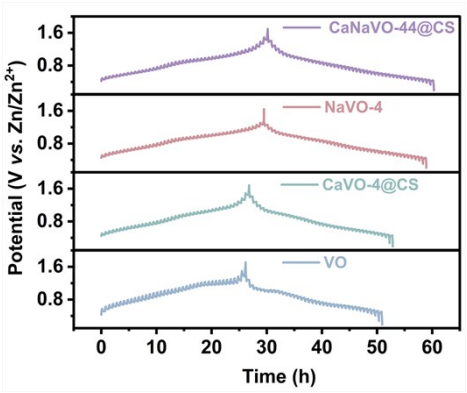

Figure S34. GITT curves after 30 min of relaxation of Zn||CaNaVO-44@CS, Zn||NaVO-4, Zn||CaVO-4@CS, and Zn||VO cells.

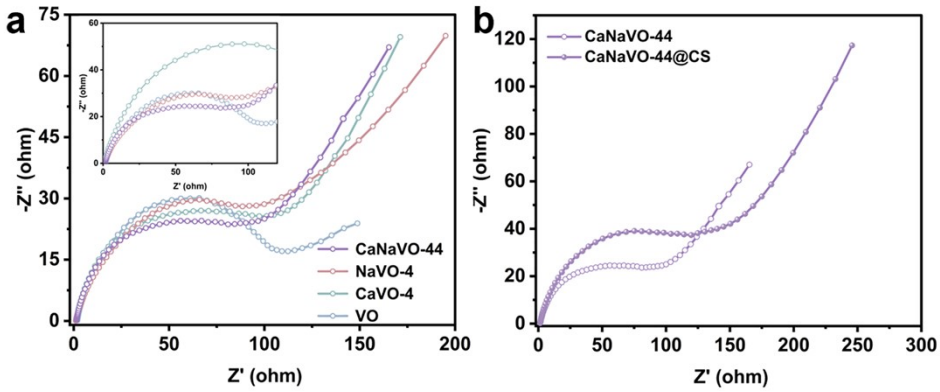

Figure S35. (a) Nyquist plots with and with an enlarged view of Nyquist plots of CaNaVO-44, NaVO-4, CaVO-4, and VO cathodes. (b) Nyquist plots of Zn||CaNaVO-44 and Zn||CaNaVO-44@CS cells.

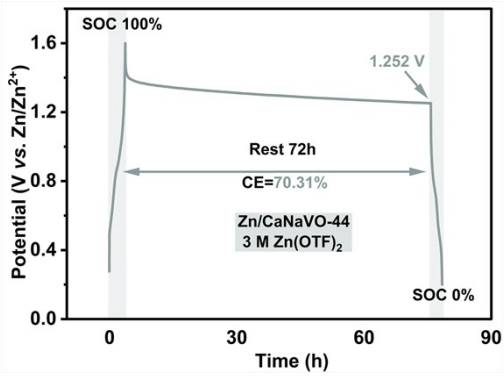

Figure S36. The self-discharge test of the Zn||CaNaVO-44@CS cell for 3 M $Zn(OTF)_2$ + 0.1 M $ZnSO_4$ electrolyte.

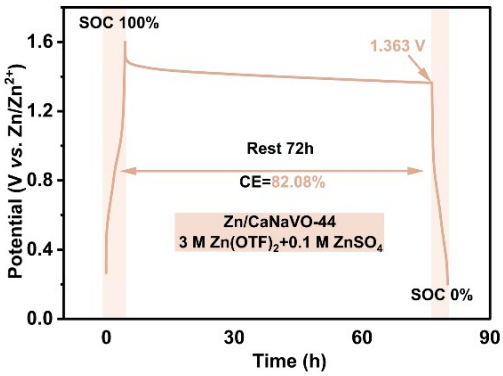

Figure S37. The self-discharge test of the Zn||CaNaVO-44@CS cell for 3 M $Zn(OTF)_2$ + 0.1 M $ZnSO_4$ electrolyte.

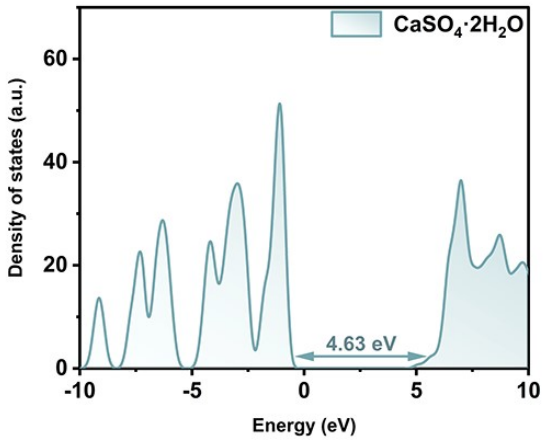

Figure S38. The density of states corresponding to $CaSO_4 \cdot 2H_2O$.

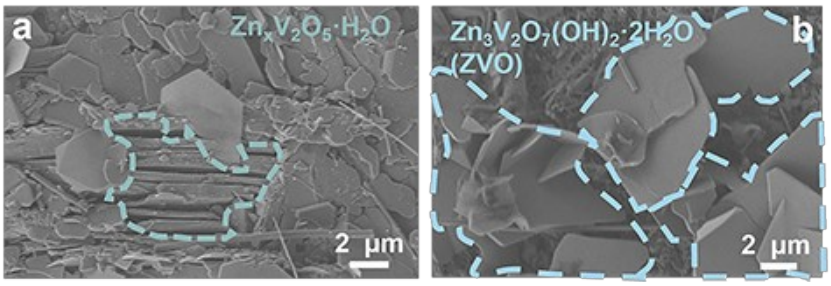

Figure S39. SEM images of CaNaVO-44@CS cathode after cycling.

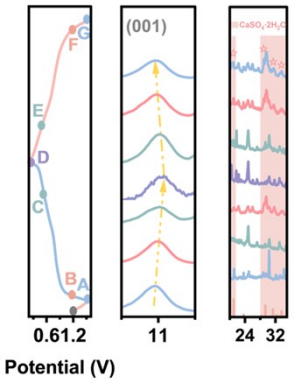

Figure S40. Specified Zn||CaNaVO-44@CS cell charging and discharging state at 25°C *ex-situ* XRD local magnification pattern.

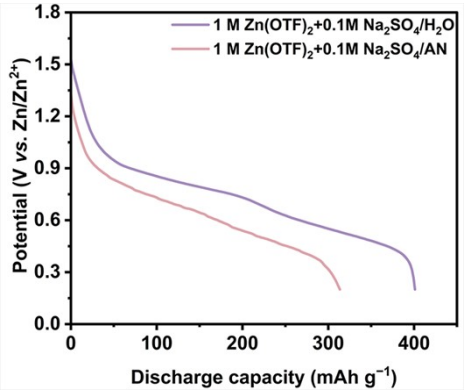

Figure S41. Discharge curves comparison of Zn||CaNaVO-44@CS cells for electrolytes using water and acetonitrile as solvents at 0.1 A g^{-1}.

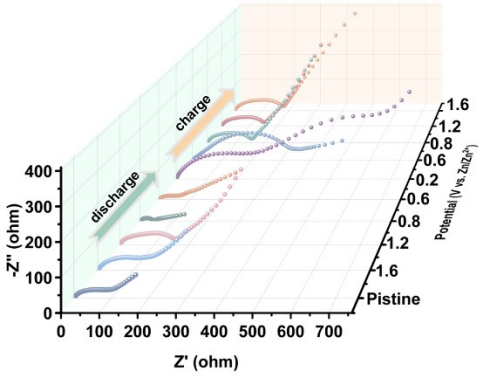

Figure S42. *In situ* EIS spectra of Zn||CaNaVO-44@CS cell.

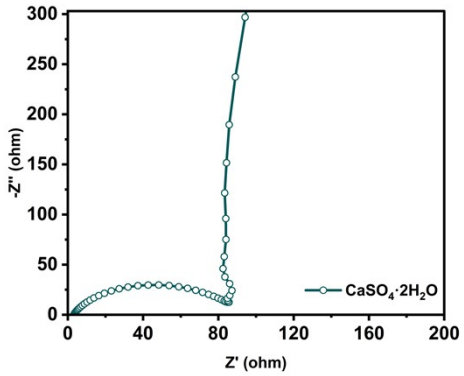

Figure S43. Nyquist plots of $CaSO_4{\cdot}2H_2O$ electrode.

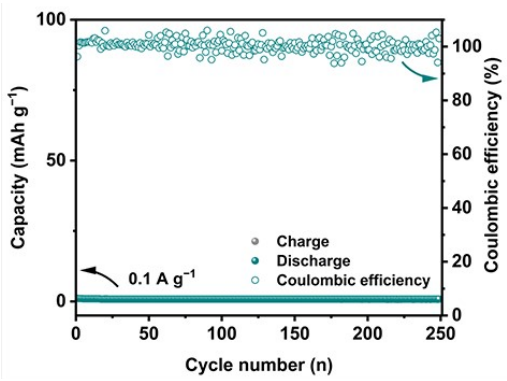

Figure S44. Cycling performance of $CaSO_4{\cdot}2H_2O$ electrode at 0.1 A g^{-1}.

CR2025-type coin cells were used for all electrochemical measurements. The $CaSO_4{\cdot}2H_2O$, super P and polyvinylidene fluoride (PVDF) binder were mixed with N-methyl-2-pyrrolidone (NMP) solvent to form a homogeneous slurry in a weight ratio of 7:2:1 to obtain the working electrode. The paste was subsequently coated onto a Ti foil (200 μm) and then dried under vacuum oven conditions at 60°C for 12 h. The resulting electrode was ultimately cut into discs with a 15 mm diameter. The total weight of $CaSO_4{\cdot}2H_2O$ on the working electrodes was trolled to be around 1 mg cm^{-2}. The AZIBs were assembled using metallic zinc foil (Φ = 15 mm) as the

anode and glass fiber (GF/F, Whatman) as the separator. The electrolyte comprised an aqueous solution of 3 M $Zn(CF_3SO_3)_2$ and 0.1 M Na_2SO_4. Electrochemical impedance spectroscopy (EIS) was conducted in the frequency range of 100 kHz to 0.1 Hz using a current amplitude of 10 mV on the Princeton PARSTAT MC 1000 electrochemical workstation.

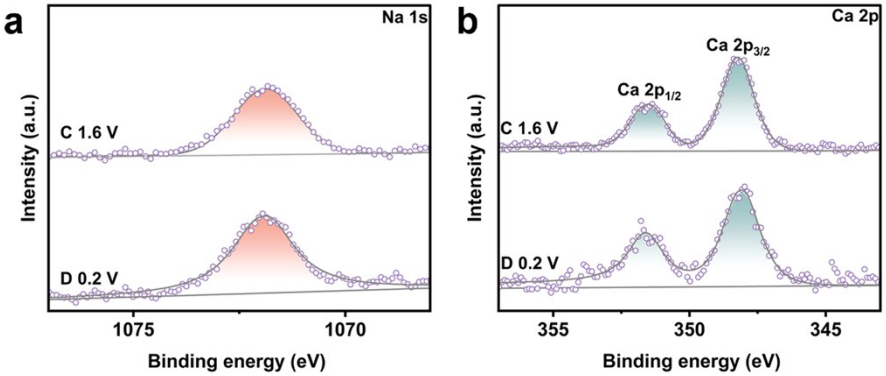

Figure S45. *Ex situ* XPS spectrums of Na 1s (a), and Ca 2p (b) of CaNaVO-44@CS cathode.

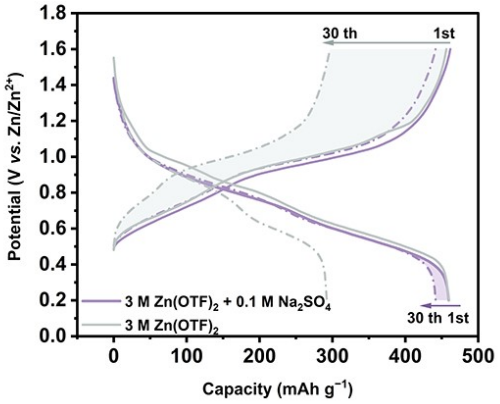

Figure S46. GCD curves of the CaNaVO-44 cathode in 3 M $Zn(OTF)_2$ and 3 M $Zn(OTF)_2$ + 0.1 M Na_2SO_4 electrolytes at 0.1 A g^{-1}.

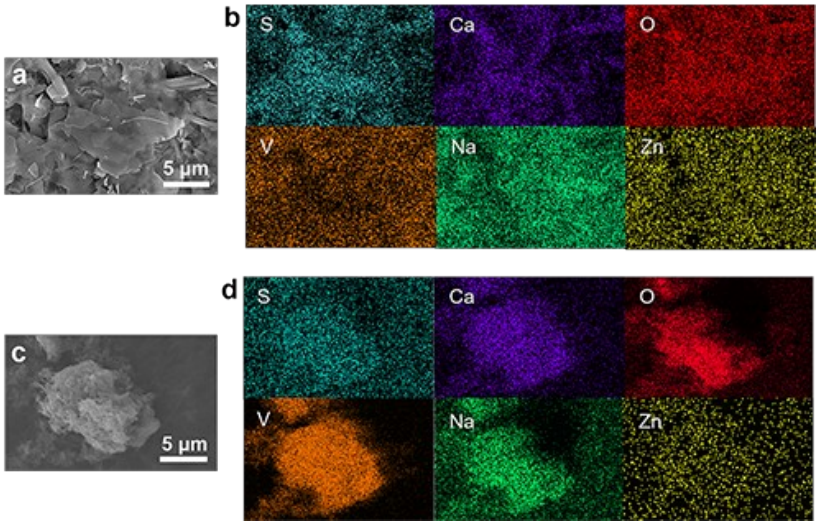

Figure S47. SEM images of CaNaVO-44@CS cathodes (a) discharged to 0.2 V, and (c) charged to 1.6 V. EDS mapping of CaNaVO-44@CS cathodes (b) discharged to 0.2 V, and (d) charged to 1.6 V.

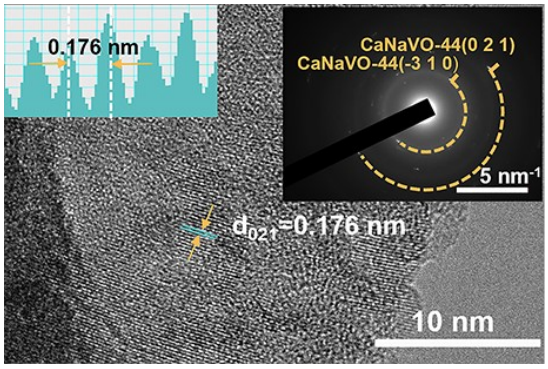

Figure S48. HRTEM image with inserted SAED pattern of CaNaVO-44 cathode after cycling without the additive Na_2SO_4.

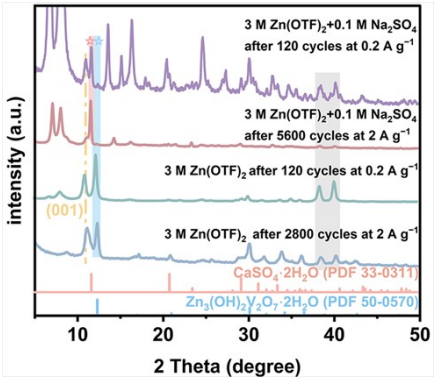

Figure S49. *Ex situ* XRD images of CaNaVO-44 cathodes after long cycling with or without additive Na_2SO_4.

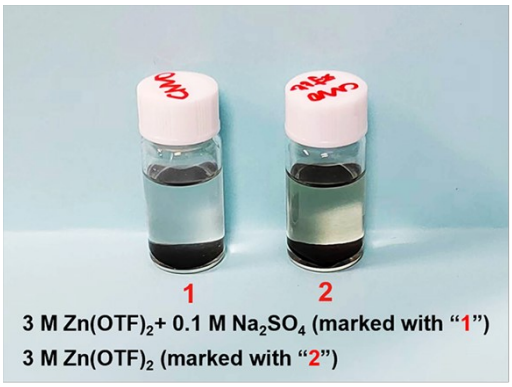

Figure S50. Optical image of CaNaVO-44 cathodes after pre-charging in 3 M $Zn(CF_3SO_3)_2$ + 0.1 M Na_2SO_4 (labeled "1") and 3 M $Zn(CF_3SO_3)_2$ (labeled "2") electrolytes after 3 days immersion in 3 M $Zn(CF_3SO_3)_2$ electrolyte.

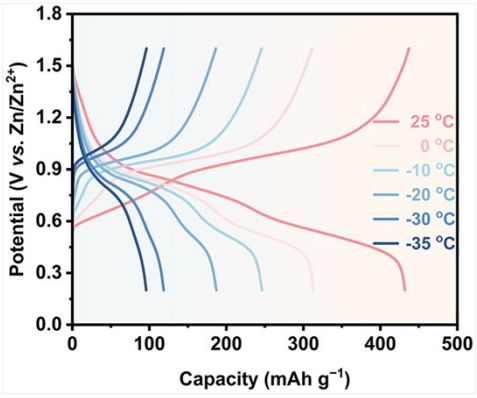

Figure S51. GCD curves of Zn||CaNaVO-44@CS cell at 0.1 A g^{-1} and 25 to -35 °C.

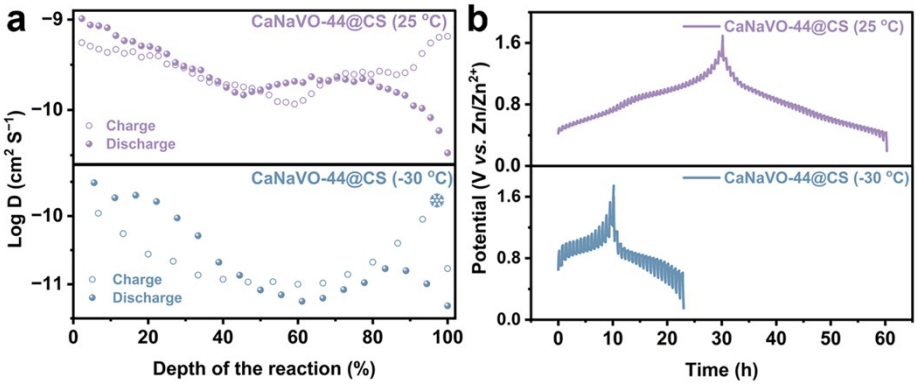

Figure S52. (a) Diffusion coefficients (Log D) corresponding to the CaNaVO-44@CS cathode at 0.05 A g^{-1} and 25, -30 °C and (b) GITT curves after 30 min of relaxation.

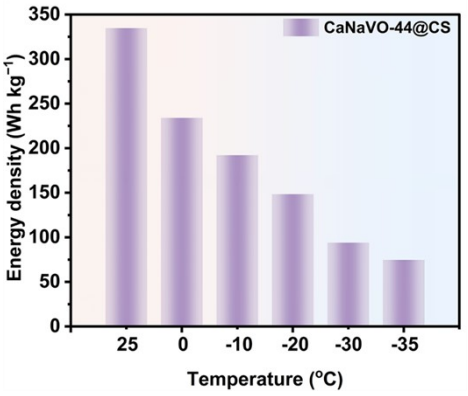

Figure S53. Energy densities of the Zn||CaNaVO-44@CS cell at 25 to -35 °C

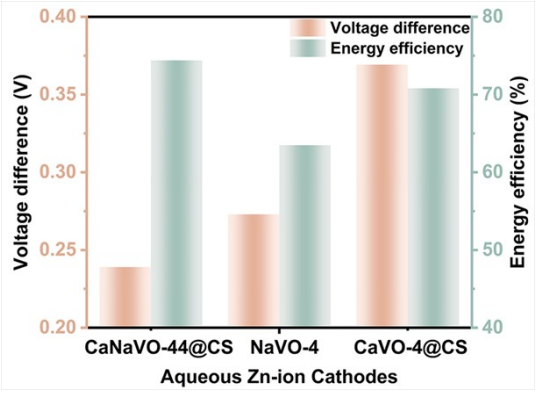

Figure S54. Differential charge and discharge voltages and energy efficiencies at 0.1 A g^{-1} and -30°C of Zn||CaNaVO-44@CS, Zn||NaVO-4 and Zn||CaVO-4@CS cells.

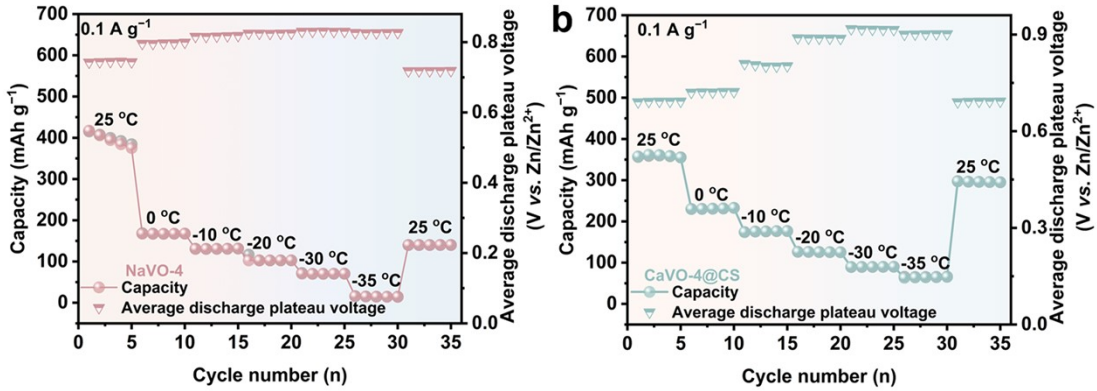

Figure S55. Capacities and average discharge voltages at 25 to -35 °C of Zn||NaVO-4 and Zn||CaVO-4@CS cells.

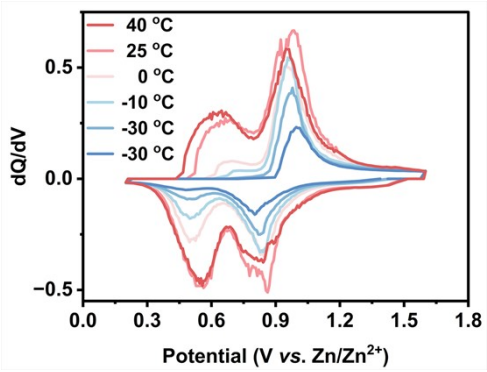

Figure S56. DQ/dV curves at 40 to -30 °C of Zn||CaNaVO-44@CS cell at 0.1 A g^{-1}.

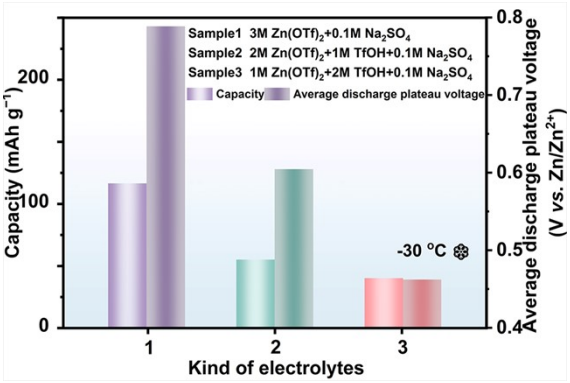

Figure S57. Capacities and average discharge voltages at 0.1 A g^{-1} and -30 °C of Zn||CaNaVO-44@CS cells with different electrolytes.

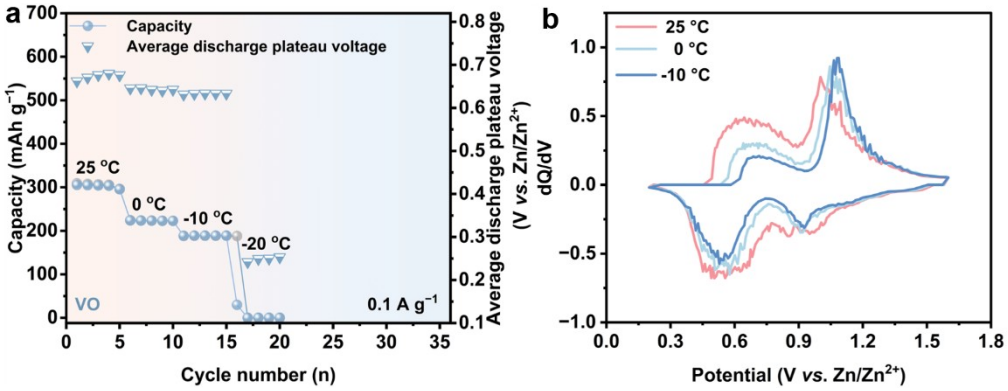

Figure S58. (a) Capacity and average discharge voltage and (b) dQ/dV curves of Zn||VO cells at 0.1 A g^{-1} at 25 to -10 °C.

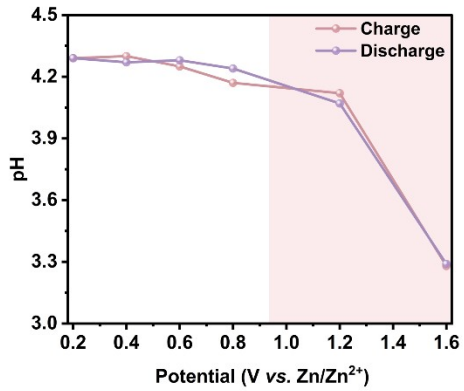

Figure S59. pH change results at 25 °C at selected charge/discharge states of Zn||VO cells.

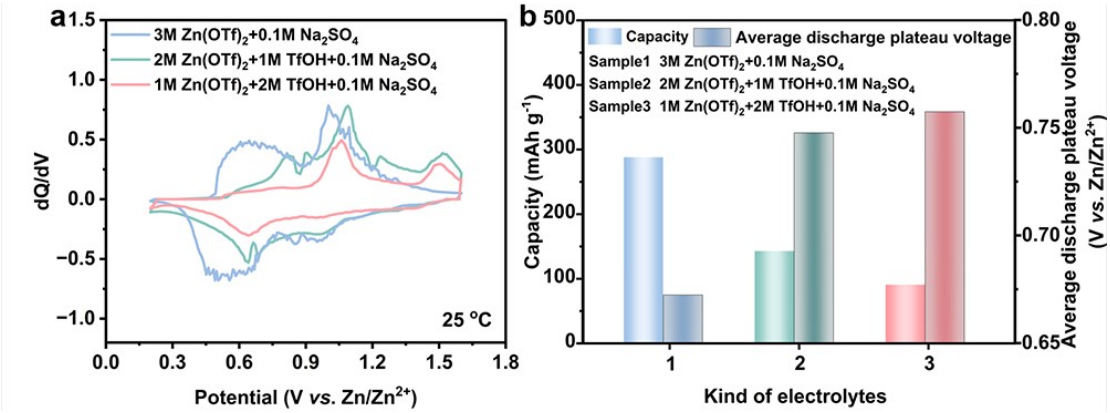

Figure S60. (a) DQ/dV curves and (b) capacities and average discharge voltages at 0.1 A g^{-1} and 25 °C of Zn||VO cells with different electrolytes.

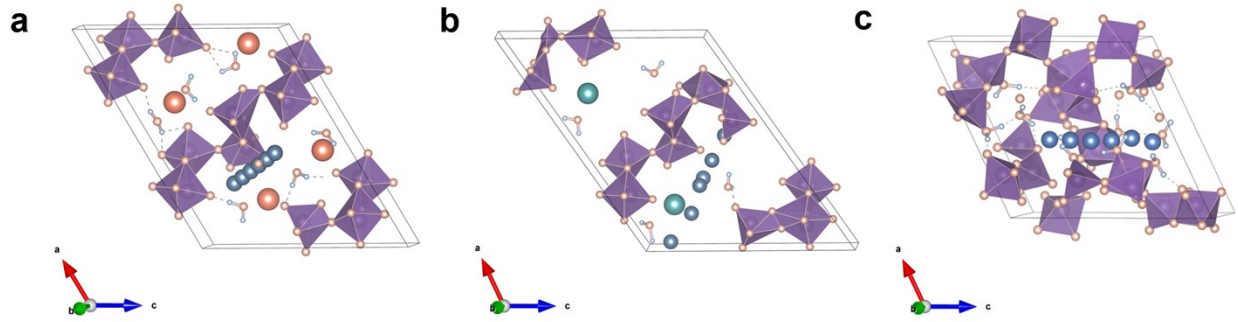

Figure S61. (a) The potential paths for the diffusion of Zn^{2+} in NaVO-44, (b)CaVO-4 and (c) VO.

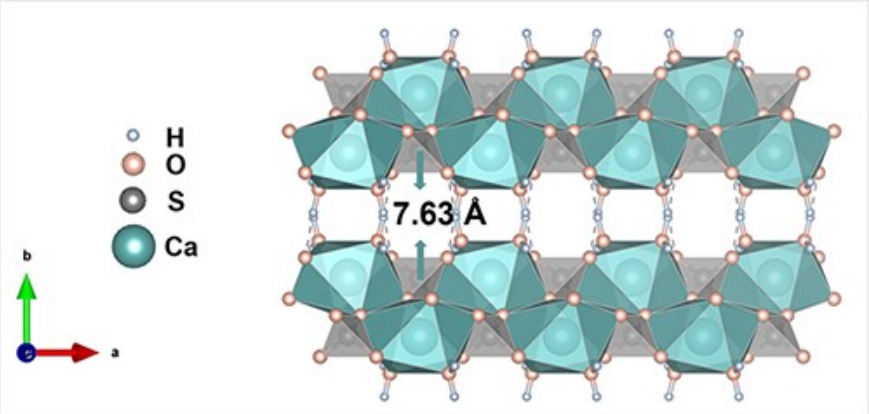

Figure S62. Crystal structure illustration of $CaSO_4 \cdot 2H_2O$.

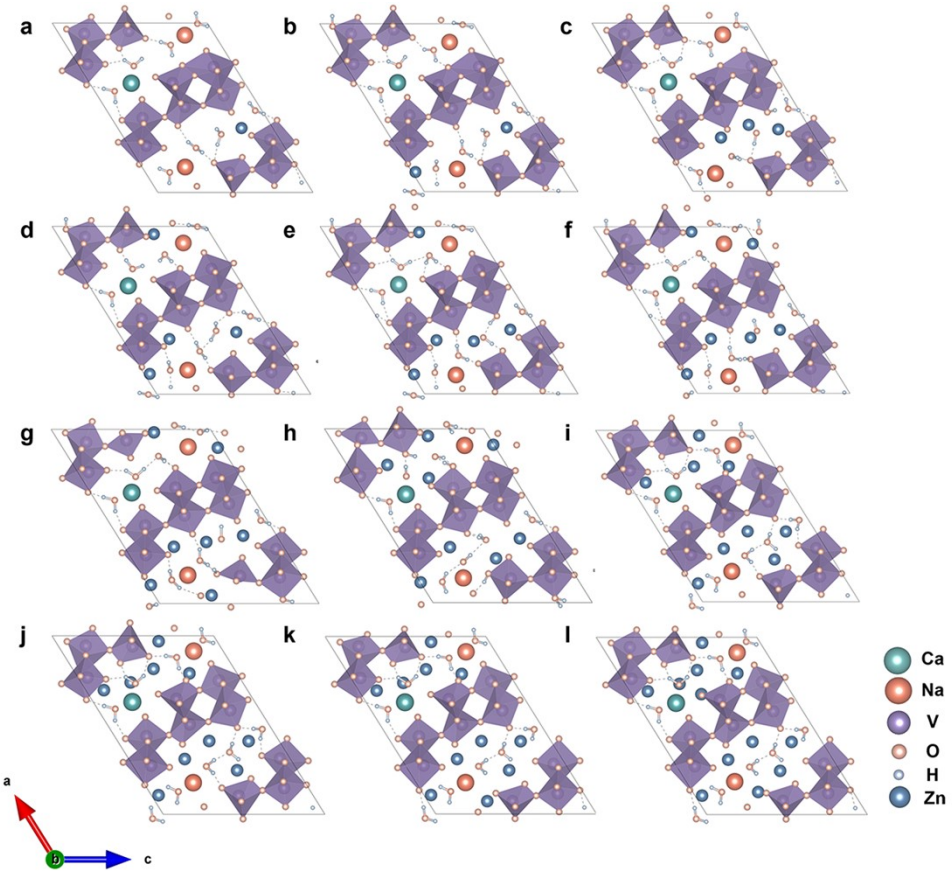

Figure S63. Structural optimization of $Zn_xCaNa_2V_{12}O_{36} \cdot 8H_2O$ (x = 1~12).

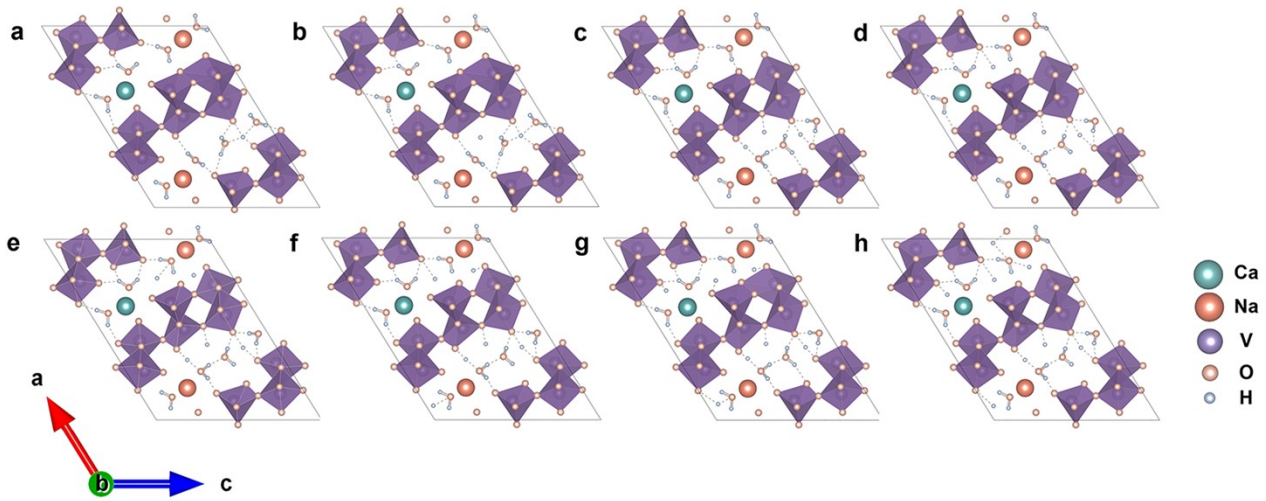

Figure S64. Structural optimization of $H_xCaNa_2V_{12}O_{36}{\cdot}8H_2O$ (x = 1~8).

Supplementary Tables

Table S1. The levels of Ca, Na, and V elements in various states of CaNaVO-44 were measured by ICP-OES techniques.

Sample	Ca	Na	V
CaNaVO-44 (pristine)	3.95%	3.90%	44.13%
CaNaVO-44 (pre-charge 1.6 V, 3 M $Zn(CF_3SO_3)_2$ + 0.1 M Na_2SO_4)	0.28%	0.29%	3.19%
CaNaVO-44 (pre-charge 1.6 V, 3 M $Zn(CF_3SO_3)_2$)	0.20%	0.19%	2.71%

Table S2. Calculated interlayer binding energies for CaNaVO-44 and VO.

Sample	Interlayer binding energy/ meV $Å^{-2}$
CaNaVO-44	-229.23
VO	-19.55

Table S3. Comparison of the electrochemical properties of the current study with other cathodes based on vanadium.

Cathode material	Electrolyte	Specific capacity	Capacity retention	Ref.
CaNaVO-44@CS	**3 M $Zn(CF_3SO_3)_2$ + 0.1 M Na_2SO_4**	**460.2 mAh g^{-1} at 0.1 A g^{-1}**	**92.7% retained after 160 cycles at 0.1 A g^{-1}** **99.4% retained after 120 cycles at 0.2 A g^{-1}** **90.1% retained after 5600 cycles at 2.0 A g^{-1}** **96.1% retained after 10000 cycles at 5.0 A g^{-1}**	**This work**
CaKVO-26@CS	**3 M $Zn(CF_3SO_3)_2$ + 0.1 M K_2SO_4**	**445.4 mAh g^{-1} at 0.1 A g^{-1}**	**90.6% retained after 100 cycles at 0.2A g^{-1}** **91.4% retained after 2400 cycles at 2.0A g^{-1}**	**This work**
BaKVO-17@BS	**3 M $Zn(CF_3SO_3)_2$ + 0.1 M K_2SO_4**	**354.8 mAh g^{-1} at 0.1 A g^{-1}**	**92.4% retained after 100 cycles at 0.2A g^{-1}** **91.8% retained after 2400 cycles at 2.0A g^{-1}**	**This work**
Li@MnVO	3 M $Zn(CF_3SO_3)_2$	375.3 mAh g^{-1} at 0.1 A g^{-1}	92.1% retained after 5000 cycles at 10.0 A g^{-1}	12

$K_2Zn_2V_{10}O_{28}$	3 M $Zn(CF_3SO_3)_2$	223.4 mAh g^{-1} at 0.1 A g^{-1}	97.6% retained after 50 cycles at 0.1 A g^{-1}	[13]
(Na, Mn)$V_8O_{20}\cdot nH_2O$	3 M $Zn(CF_3SO_3)_2$	377 mAh g^{-1} at 0.1 A g^{-1}	88% retained after 1000 cycles at 4.0 A g^{-1}	[14]
$([N(CH_3)_4]_{0.77},Zn_{0.23})V_8O_{20}\cdot 3.8H_2O$	3 M $Zn(CF_3SO_3)_2$	301.4 mAh g^{-1} at 0.2 A g^{-1}	80.2% retained after 6000 cycles at 8.0 A g^{-1}	[15]
$Ba_{1.2}V_6O_{16}\cdot 3H_2O$	2 M $ZnSO_4$	321.2 mAh g^{-1} at 0.1 A g^{-1}	95.6% retained after 2000 cycles at 5.0 A g^{-1}	[16]
LiV_3O_8	3 M $Zn(CF_3SO_3)_2$	450 mAh g^{-1} at 0.1 A g^{-1}	85% retained after 4000 cycles at 5.0 A g^{-1}	[17]
$K_2V_6O_{16}\cdot 2.7H_2O$	3 M $Zn(CF_3SO_3)_2$	367 mAh g^{-1} at 0.1 A g^{-1}	93% retained after 1000 cycles at 1.0 A g^{-1}	[18]
$Na_xVO_2\cdot 0.3H_2O$	2 M $ZnSO_4$	397 mAh g^{-1} at 0.2 A g^{-1}	90.1% retained after 3000 cycles at 12.0 A g^{-1}	[19]
$Na_{0.5}K_{0.5}VO$	3 M $ZnSO_4$	393 mAh g^{-1} at 0.1 A g^{-1}	99.2% retained after 100 cycles at 0.5 A g^{-1}	[20]
LVO@NVO	3 M $ZnSO_4$	476 mAh g^{-1} at 0.05 A g^{-1}	93.4% retained after 2000 cycles at 5.0 A g^{-1}	[21]
KMgVOH	3 M $Zn(CF_3SO_3)_2$	423 mAh g^{-1} at 0.1 A g^{-1}	72% retained after 2000 cycles at 4.0 A g^{-1}	[22]

Table S4. The levels of Ca elements in various states of CaNaVO-44@CS were measured by ICP-OES techniques.

Sample	Ca Concentration (mg/L)
CaNaVO-44@CS (charge 1.6 V)	0.73
CaNaVO-44@CS (discharge 0.2 V)	0.83

Table S5. Concentration of Ca^{2+} in 3M $Zn(CF_3SO_3)_2$ electrolyte at different pH conditions.

pH	Ca^{2+} concentration (mg/L)
3.0	8.138
3.4	7.452
3.8	6.121
4.2	3.554

50 mg of $CaSO_4{\cdot}2H_2O$ were added to 10 ml of 3M $Zn(CF_3SO3)_2$ electrolyte with pH values of 3.0, 3.4, 3.8, and 4.2, respectively. The mixture was stirred for 12 h and then filtered through a 0.22 μm filter membrane before being used for ICP-OES measurements.

Table S6. V content after immersing the cathodes in 3M $Zn(CF_3SO_3)_2$ electrolyte for three days for CaNaVO-44 cathodes with $CaSO_4{\cdot}2H_2O$ CEI and without $CaSO_4{\cdot}2H_2O$ CEI measured by ICP-OES techniques.

Sample	V Concentration (mg/L)
CaNaVO-44 with $CaSO_4{\cdot}2H_2O$ CEI	0.44
CaNaVO-44 without $CaSO_4{\cdot}2H_2O$ CEI	5.20

Table S7. Performance comparison of the Zn||CaNaVO-44@CS cell in this work with typical low-temperature batteries reported in the literature.

System	Cathode material	Electrolyte	Current density	Capacity retention	Ref.
AZIBs	**CaNaVO-44@CS**	**3 M $Zn(CF_3SO_3)_2$ + 0.1 M Na_2SO_4**	**0.1 A g^{-1}**	**84.5% retained after 1000 cycles at -30°C**	**This work**
	CaNaVO-44@CS	**3 M $Zn(ClO_4)_2$ + 0.1 M Na_2SO_4**	**0.1 A g^{-1}**	**90.8% retained after 2000 cycles at -30°C**	**This work**
LIBs	NMC811	TCE	C/3	80.7% retained after 700 cycles at -20°C	23
	NCM523	1 M $LiPF_6$ in EC/DMC/EMC	0.1 C	86.6% retained after 300 cycles at -10°C	24
	NMC532	1.0 M LiFSI / (DiFEC: MTFC: HFME, 1:2:2 vol%)+50 mM NaFSI	0.2 C	72.2% retained after 92 cycles at -20°C	25
	NMC111	1 M LiPF6 / (MP: FEC, 9:1 vol%)	0.2 C	92% retained after 100 cycles at -20°C	26
SIBs	$Na_3V_2(PO_4)_3$	1 M $NaPF_6$-G2/DME	0.5 C	80.6% retained after 1400 cycles at -40°C	27
	$Na_3V_2(PO_4)_3$	ES6-BLTE	0.1 C	88.2% retained after 200 cycles at -40°C	28

MLIBs	1T-VSe_2	0.1 M MACC + of 1.0 M LiCl	0.1 A g^{-1}	97% retained after 500 cycles at -20°C	[29]
AZIBs	MnO_2	3 M $Zn(ClO_4)_2$	1.0 C	80% retained after 1000 cycles at -30°C	[30]
	O_d-VO_2-rG	1 M $ZnSO_4$ + DES: H_2O (1:1)	0.1 A g^{-1}	75 % retained after 1100 cycles at -40°C	[31]
	V_2O_5	2 M $Zn(CF_3SO_3)_2$	0.5 A g^{-1}	81.7% retained after 1000 cycles at -30°C	[32]
	V_2O_5	1M $Zn(CF_3SO_3)_2$ + 0.15 M DME	0.2 A g^{-1}	~78.8% retained after 1000 cycles at -40°C	[33]
	TCBQ	4 M $Zn(BF_4)_2$	0.22 A g^{-1}	94% retained after 1000 cycles at -30°C	[34]

Table S8. Molar stoichiometric ratios of Zn/V for specified CaNaVO-44@CS cathodes discharge states as quantified by ICP−OES.

Sample	Zn/V
Pristine	0
Discharged to 1.2 V (vs. Zn/Zn^{2+})	0.036
Discharged to 0.6 V (vs. Zn/Zn^{2+})	0.592
Discharged to 0.2 V (vs. Zn/Zn^{2+})	1.112

References:

1. G. Kresse and J. Hafner, *Phys. Rev. B*, 1993, **47**, 558-561.
2. G. Kresse and J. Furthmüller, *Comp. Mater. Sci.*, 1996, **6**, 15-50.
3. G. Kresse, *Phys. Rev. B Condens. Matter*, 1999, **59**, 1758-1775.
4. K. Zhu, T. Wu and K. Huang, *Adv. Energy Mater.*, 2019, **9**, 1901968.
5. Y. Huang, P. Zhu, C. Gu, H. Xu, J. Zhou and G. Xiao, *J. Energy Storage*, 2023, **73**, 108804.
6. W. Yang, L. Xu, W. Luo, M. Huang, K. Fu, R. Song, C. Han, R. Tu, J. Shi and L. Mai, *Matter*, 2023, **6**, 3006-3020.
7. T. He, Y. Ye, H. Li, S. Weng, Q. Zhang, M. Li, T. Liu, J. Cheng, X. Wang, J. Lu and B. Wang, *Mater. Today*, 2021, **43**, 53-61.
8. J. Li, N. Luo, L. Kang, F. Zhao, Y. Jiao, T. J. Macdonald, M. Wang, I. P. Parkin, P. R. Shearing, D. J. L. Brett, G. Chai and G. He, *Adv. Energy Mater.*, 2022, **12**, 2201840.
9. Y. Wang, S. Wei, Z.-H. Qi, S. Chen, K. Zhu, H. Ding, Y. Cao, Q. Zhou, C. Wang, P. Zhang, X. Guo, X. Yang, X. Wu and L. Song, *Proc. Natl. Acad. Sci. U.S.A.*, 2023, **120**, e2217208120.
10. Y. Chen, Q. He, Y. Zhao, W. Zhou, P. Xiao, P. Gao, N. Tavajohi, J. Tu, B. Li, X. He, L. Xing, X. Fan and J. Liu, *Nat. Commun.*, 2023, **14**, 8326.
11. D. Wang, C. Li, Q. Li, H. Li, J. Rehman, C. Zhi and L. Zhu, *Nano Energy*, 2022, **104**, 107990.
12. H. Jiang, Y. Zhang, M. Waqar, J. Yang, Y. Liu, J. Sun, Z. Feng, J. Sun, Z. Pan, C. Meng and J. Wang, *Adv. Funct. Mater.*, 2023, **33**, 2213127.
13. T. Zhou, L. Zhu, L. Xie, Q. Han, X. Yang, X. Cao and J. Ma, *Small*, 2022, **18**, 2107102.
14. M. Du, C. Liu, F. Zhang, W. Dong, X. Zhang, Y. Sang, J.-J. Wang, Y.-G. Guo, H. Liu and S. Wang, *Adv. Sci.*, 2020, **7**, 2000083.
15. F. Zhang, X. Sun, M. Du, X. Zhang, W. Dong, Y. Sang, J. Wang, Y. Li, H. Liu and S. Wang, *Energy Environ. Mater.*, 2021, **4**, 620-630.
16. X. Wang, B. Xi, X. Ma, Z. Feng, Y. Jia, J. Feng, Y. Qian and S. Xiong, *Nano Lett.*, 2020, **20**, 2899-2906.
17. P. He, M. Yan, X. Liao, Y. Luo, L. Mai and C.-W. Nan, *Energy Storage Mater.*, 2020, **29**, 113-120.
18. B. Sambandam, V. Soundharrajan, S. Kim, M. H. Alfaruqi, J. Jo, S. Kim, V. Mathew, Y.-k. Sun and J. Kim, *J. Mater. Chem. A*, 2018, **6**, 15530-15539.
19. Y. Liu and X. Wu, *Nano Energy*, 2021, **86**, 106124.
20. L. Shan, Y. Wang, S. Liang, B. Tang, Y. Yang, Z. Wang, B. Lu and J. Zhou, *InfoMat*, 2021, **3**, 1028-1036.
21. J. Wang, X. Zhao, J. Kang, X. Wang, H. Yu, C.-F. Du and Q. Yan, *J. Mater. Chem. A*, 2022, **10**, 21531-21539.
22. Z. Feng, Y. Zhang, J. Sun, Y. Liu, H. Jiang, M. Cui, T. Hu and C. Meng, *Chem. Eng. J.*, 2022, **433**, 133795.
23. W. Zhang, G. Jiang, W. Zou, X. Chen, S. Peng, S. Qi, R. Hu, H. Song, Z. Cui, L. Du and Z. Liang, *Energy Environ. Sci.*, 2024, DOI: 10.1039/D3EE04458K.
24. C. Wang, Y. Xie, Y. Huang, S. Zhou, H. Xie, H. Jin and H. Ji, *Angew. Chem. Int. Ed.*, **n/a**, e202402301.
25. X. Zheng, Z. Cao, W. Luo, S. Weng, X. Zhang, D. Wang, Z. Zhu, H. Du, X. Wang, L. Qie, H. Zheng and Y. Huang, *Adv. Mater.*, 2023, **35**, 2210115.
26. Y.-G. Cho, M. Li, J. Holoubek, W. Li, Y. Yin, Y. S. Meng and Z. Chen, *ACS Energy Lett.*, 2021, **6**, 2016-2023.
27. Y. Wang, H. Lan, S. Dong, Q. Zhu, L. Cheng, H. Wang, J. Wang, S. Wang, M. Tang, K. M. Shodievich, G. Wang and H. Wang, *Adv. Funct. Mater.*, **n/a**, 2315498.
28. S. Zhong, Y. Yu, Y. Yang, Y. Yao, L. Wang, S. He, Y. Yang, L. Liu, W. Sun, Y. Feng, H. Pan, X. Rui and Y. Yu, *Angew. Chem. Int. Ed.*, 2023, **62**, e202301169.
29. X. Xu, C. Ye, D. Chao, K. Davey and S.-Z. Qiao, *Adv. Energy Mater*, 2023, **13**, 2204344.

30. S. Gao, B. Li, H. Tan, F. Xia, O. Dahunsi, W. Xu, Y. Liu, R. Wang and Y. Cheng, *Adv. Mater.*, 2022, **34**, 2201510.

31. C. Zhu, X. He, Y. Shi, Z. Wang, B. Hao, W. Chen, H. Yang, L. Zhang, H. Ji, J. Liu, C. Yan, J. Zhou and T. Qian, *ACS Nano*, 2023, **17**, 21614-21625.

32. Q. Zhang, K. Xia, Y. Ma, Y. Lu, L. Li, J. Liang, S. Chou and J. Chen, *ACS Energy Lett.*, 2021, **6**, 2704-2712.

33. Y. Dong, N. Zhang, Z. Wang, J. Li, Y. Ni, H. Hu and F. Cheng, *J. Energy Chem.*, 2023, **83**, 324-332.

34. T. Sun, X. Yuan, K. Wang, S. Zheng, J. Shi, Q. Zhang, W. Cai, J. Liang and Z. Tao, *J. Mater. Chem. A*, 2021, **9**, 7042-7047.